Chapter 7
A Review of the Class of Bouc-Wen Differential Models for Simulating Mechanical Hysteresis Phenomena

Davide Pellecchia and Massimo Paradiso

Abstract One of the most popular hysteretic models used in many areas of engineering, especially the civil one, is the Bouc-Wen model. Although this model is able to simulate several types of hysteretic phenomena, it cannot describe some typical phenomena, such as cyclic degradation of strength and stiffness, pinching effect, and so on. For this reason, many researchers have proposed several variants of the original Bouc-Wen model. We present a review of the Bouc-Wen model and its most significant enhanced versions, utilizing the same technical terminology for all models in order to clarify and to shed some light on the number and physical significance of the parameters that the models require as input. Sensitivity analyses are also illustrated with respect to the input parameters.

Keywords Civil engineering · Hysteresis · Bouc-Wen model · Cyclic degradation · Sensitivity analysis

7.1 Introduction

Hysteresis is a complex phenomenon that can be experienced in many fields of science and technology; undoubtedly it represents the predominant typology of nonlinear constitutive behavior. The importance of properly reproducing hysteretic responses in engineering has been highlighted by several contributions available in the literature (Visintin 2013). The main research fields include civil applications (Bahn and Hsu 1998; Lima et al. 2018; Zuccaro et al. 2017), magnetism (Bai et al. 2019), as well as higher-gradient materials (Alibert et al. 2003; Pideri and Seppecher 1997; Barchiesi et al. 2018), and mechanics of thermal and porous media (Altenbach et al.

D. Pellecchia (✉) · M. Paradiso
Department of Structures for Engineering and Architecture, University of Naples Federico II, via Claudio 21, 80125 Naples, Italy
e-mail: davide.pellecchia@unina.it

M. Paradiso
e-mail: massimo.paradiso@unina.it

F. Marmo et al. (eds.), *Mathematical Applications in Continuum and Structural Mechanics*, Advanced Structured Materials 127,
https://doi.org/10.1007/978-3-030-42707-8_7

2012; Eremeyev and Morozov 2010). Beyond basic applications such as the modeling of seismic devices (Kikuchi and Aiken 1997), dampers (Nuzzo et al. 2019), and concrete (Sessa et al. 2018, 2019b), hysteresis plays a significant role also for the analysis of more complex mechanical systems (Badoni and Makris 1996; Song et al. 2007; Greco and Cuomo 2013) including applications concerning framed (Marmo et al. 2011; Marmo and Rosati 2012a, b, 2013) and shell structures (Caggegi et al. 2018; Serpieri et al. 2018; Ascione et al. 2017; Sessa et al. 2017, 2019a; Valoroso et al. 2014, 2015), structural identification (Noël and Kerschen 2017), and random vibrations (Baber and Noori 1985; Sessa 2010; Wen 1976). More recent developments concerns meta-materials (Turco et al. 2017, 2018; De Angelo et al. 2019; di Cosmo et al. 2018; Andreaus et al. 2018) based on pantographic microstructures (Barchiesi et al. 2020; dell'Isola et al. 2019a, 2019b; Nejadsadeghi et al. 2019) as well as the modeling of damage (Contrafatto and Cuomo 2002; Contrafatto et al. 2012; Placidi et al. 2018, 2019).

The output of hysteretic systems and materials typically depends on present and past histories of the input variable and can exhibit different peculiar features: in particular, when the first time derivative of the input variable does not influence the output, this hysteresis phenomenon is denominated *rate-independent*.

The development of mathematical models able to describe such nonlinear phenomena is very complicated. In particular, in the last few years, many researchers have proposed different models whose common objective was not to explain the physical origin of the hysteresis but to try to reproduce the overall experimental behavior (Mayergoyz 2003). These models are called *phenomenological* models.

It is possible to classify the phenomenological models according to the nature of the equation to solve for the evaluation of the output variable, namely the generalized force or the generalized displacement. In particular one has:

- algebraic models, such as the ones developed by Ramberg and Osgood Ramberg and Osgood (1943), Menegotto and Pinto Menegotto (1973), and Vaiana et al. (2019a, b, c, 2020, 2021b, a, c);
- trascendental models, such as the ones introduced by Kikuchi and Aiken Kikuchi and Aiken (1997) and Sessa et al. (2020); Vaiana et al. (2018);
- differential models, such as those formulated by Bouc (1967, 1971), Özdemir Özdemir (1976), and Wen (1976, 1980);
- damage-based models, such as the one proposed by Fedele et al. (2012), Sessa and Valoroso (2017), Valoroso and Fedele (2010), Valoroso et al. (2013).

Among existing models, the differential ones are currently the most used models to reproduce the behavior of mechanical systems and materials. These models are typically based on the Duhem hysteresis operator (Duhem 1897) whose formulation is defined by a Cauchy problem of the form:

$$\begin{cases} \dot{z}(t) = g_1(x, z)\, \dot{x}(t)^+ + g_2(x, z)\, \dot{x}(t)^-, \\ z(0) = z_0, \end{cases} \tag{7.1}$$

in which $z(t)$ and $x(t)$ denote the hysteretic functions and the generalized displacement, respectively, and the superimposed dot denotes the derivative with respect to time t; g_1 and g_2 are continuous functions whereas $\dot{x}(t)^+ = \max(0, \dot{x}(t))$ and $\dot{x}(t)^- = \min(0, \dot{x}(t))$; finally z_0 represents the value of the function $z(t)$ at the time $t = 0$. All models based on Duhem's class are characterized by a peculiar property: the output value can be evaluated if the current values of the input and output variables (x, z) as well as the sign of the first derivative with respect to time of the input variable $(\text{sign}(\dot{x}))$ are known Dimian and Andrei (2014). Examples of differential models based on the Duhem hysteresis operator are the ones proposed by Jiles and Atherton (1983, 1984), Hodgdon (1988), Bouc (1971), Wen (1976, 1980), and Özdemir (1976).

The present work aims to illustrate the evolution of the Bouc-Wen model in the area of mechanics. In particular, such an evolution is described with reference to the modeling of symmetric and asymmetric hysteresis loops, hysteresis loops with pinching, and hysteresis loops with strength and/or stiffness degradation typically displayed by *rate-independent* mechanical systems and materials. The influence of the input parameters on the dimension and/or shape of the hysteresis loops is shown and discussed for each hysteretic model.

This paper is organized into four parts. In Sect. 7.2, we review some models able to describe symmetric hysteresis behaviors, namely the Bouc model (Bouc 1967, 1971) and the Wen model (Wen 1976), the latter currently known as the Bouc-Wen model. In Sect. 7.3, we review some modified Bouc-Wen models able to describe asymmetric hysteresis behaviors. In Sect. 7.4, the modified versions of the Bouc-Wen model, proposed by some researchers in order to account for the pinching effect, are illustrated. Finally, in Sect. 7.5, some models able to simulate both the strength and stiffness degradation are described.

7.2 Modeling of Symmetric Hysteresis Loops

From a mathematical point of view, symmetric hysteresis loops are characterized by odd functions with respect to the origin of the reference frame, i.e. hysteretic functions z fulfilling the condition

$$z(x) = -z(-x). \tag{7.2}$$

Among several mechanical systems and materials that exhibit a nonlinear behavior characterized by symmetric hysteresis loops, we recall, as an example, the typical cross section of steel and concrete filled steel elements (Colombo and Negro 2005; Shih and Sung 2005), metal devices, such as wire rope isolators deforming along their transverse directions (Vaiana et al. 2017), and seismic protection devices, such as isolators (Greco et al. 2018; Hadad et al. 2017; Losanno et al. 2019a, b, 2021; Sierra et al. 2019; Vaiana et al. 2019d; Pellecchia et al. 2020) and dampers (Nuzzo et al. 2018, 2019). In Fig. 7.1, some examples of symmetric hysteresis loops obtained in experimental tests are shown.

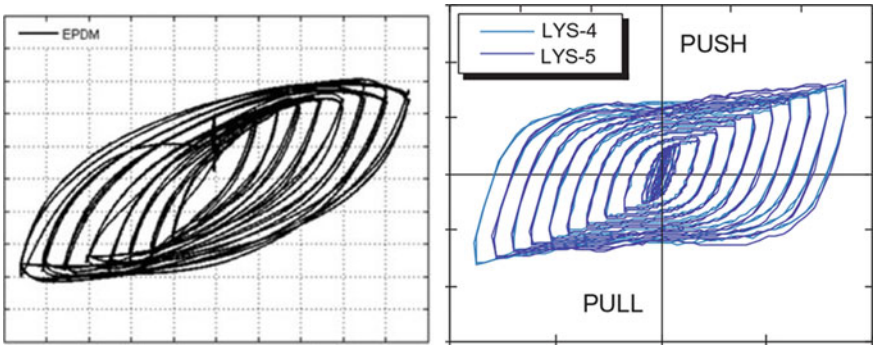

Fig. 7.1 Some symmetric hysteresis loops obtained in experimental tests. **a** The hysteresis behavior of a bearing—Hadad et al. (2017). **b** The hysteresis behavior of a rhombic steel plate Shih and Sung (2005)

The restoring force of the above-described mechanical systems and materials is typically computed as follows:

$$f(x) = f_e(x) + f_h(x), \tag{7.3}$$

where $f_e(x)$ is the elastic component whereas $f_h(x)$ is the hysteretic one. In turn, the restoring force can be described in the following way:

$$f(x) = \alpha\, k\, x + (1 - \alpha)\, k\, z(x), \tag{7.4}$$

in which α is ratio between the post-yield and pre-yield stiffness whereas k is defined as the stiffness at yield, i.e. the ratio between the yield force and the generalized yield displacement.

7.2.1 Bouc Model and Its Modified Versions

The full class of Bouc models is described by the following general nonlinear first-order ordinary differential equation:

$$\dot{z} = B\, \dot{x}, \tag{7.5}$$

in which $\dot{z}$ denotes the time derivative of the hysteretic variable, required to evaluate the rate-independent hysteretic component $f_h(x) = (1 - \alpha)\, k\, z(x)$, whereas $\dot{x}$ is the generalized velocity. The hysteretic function z basically depends on the system behavior, material properties, and response amplitude.

The nonlinear function B has been assumed of different forms over the years Bouc (1967, 1971):

$$\text{Bouc model 1 (1967):} \quad B = A - z\,\beta\ \text{sign}(\dot{x}), \tag{7.6a}$$

$$\text{Bouc model 2 (1967):} \quad B = A - |z|\left(\gamma + \beta\ \text{sign}(\dot{x}\,z)\right), \tag{7.6b}$$

$$\text{Wen model (1976):} \quad B = A - |z^n|\left(\gamma + \beta\ \text{sign}(\dot{x}\,z)\right) \tag{7.6c}$$

where A, n, and γ are material parameters that tune the size and/or the shape of the hysteresis loops.

Equation (7.6a), that defines the original Bouc model, is characterized by two model parameters, namely A and β. Subsequently, Bouc has modified such an equation by adding a new parameter, that is γ, as shown in Eq. (7.6b). Finally, Wen has extended the class of the Bouc differential models by adding the parameter n in order to smooth the hysteretic curve predicted by the original Bouc model. Note that equation $f(x) = \alpha\,k\,x + (1-\alpha)\,k\,z$ and Eq. (7.6c) define the so-called Bouc-Wen model.

The smooth nature of the Bouc model modified by Wen makes it particularly convenient for addressing several engineering problems especially when several dynamic analyses are required. This includes the case of flutter analysis (Carboni et al. 2018) and Random Vibration analysis of structures (Broccardo et al. 2017; Fujimura and Der Kiureghian 2007; Sessa 2010).

The Bouc-Wen model is capable of reproducing several behaviors depending on the parameters A, β, γ, and n, whose influence on the hysteretic variable z is illustrated in Sect. 7.2.2.

7.2.2 *Sensitivity Analysis*

A parameter sensitivity analysis was carried out to evaluate the effect of each parameter on the hysteretic variable $z(x)$ obtained by adopting Eqs. (7.5) and (7.6c).

The relationship between the hysteretic variable z and the generalized displacement x is shown in Fig. 7.2 for different combinations of the constitutive parameters. All hysteretic loops are obtained by applying a generalized displacement described by the following sine wave:

$$x(t) = 2\ \sin(t) \tag{7.7}$$

and integrating differential Eq. (7.5) by MATLAB ® using the solver ode45.

The top left plot shows that the tangent stiffness at the origin of the hysteresis loop increases when the parameter A is increased and its sign is the same as that of A; for negative values of parameter A, the tangent stiffness at the origin becomes negative.

The top right plot shows that the hysteretic energy dissipation increases as β increases. In particular, an elastic nonlinear constitutive law can be obtained by setting $\beta = 0$.

The bottom left plot shows that the hysteresis loop is bounded between two parallel straight lines and it rotates clockwise when the parameter γ is increased. On the other

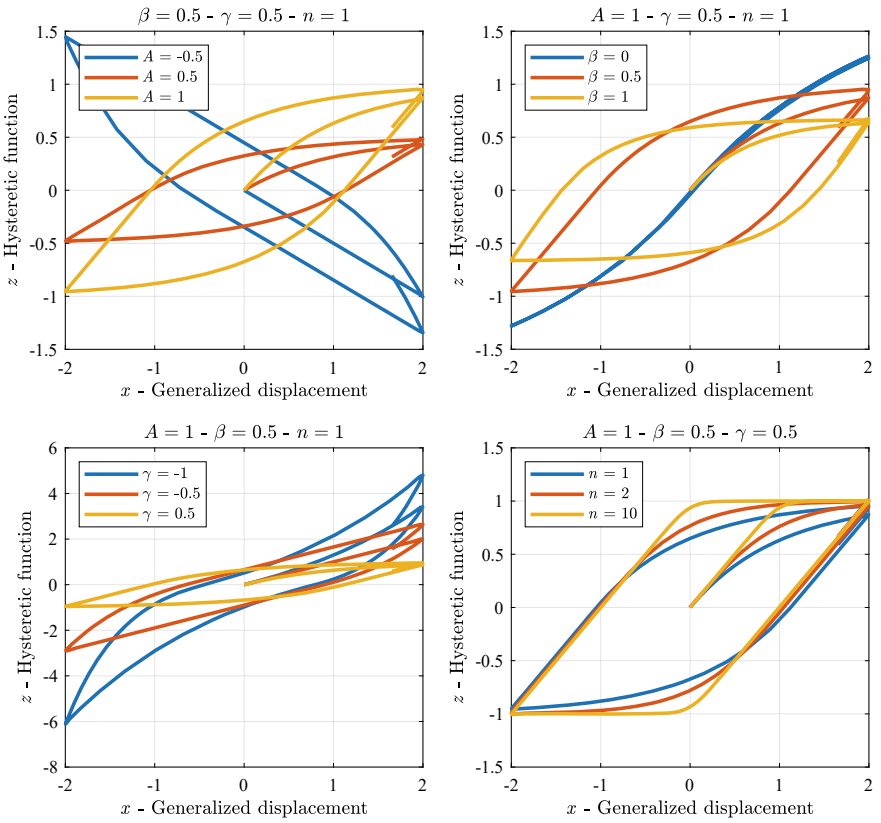

Fig. 7.2 Sensitivity analysis of the Bouc-Wen model with respect to the material parameters

hand, by decreasing the value of γ, the hysteresis loop is bounded by two parallel curves such that, for high values of the displacement x, the hysteresis loop exhibits a work hardening behavior.

Finally, the bottom right plot shows that the hysteresis loop gets smoother with decreasing n so that such a parameter can be related to the smoothness of the hysteresis loop. In the limit case $n \to \infty$, the constitutive law becomes elastic-perfectly plastic.

7.3 Modeling of Asymmetric Hysteresis Loops

There exist several mechanical systems and materials displaying a nonlinear response characterized by asymmetric hysteresis loops; typical examples are some materials, such as metals (Dobson et al. 1997), polymers (Hossain et al. 2012), and shape memory alloys (Graesser and Cozzarelli 1991), as well as some devices, such as

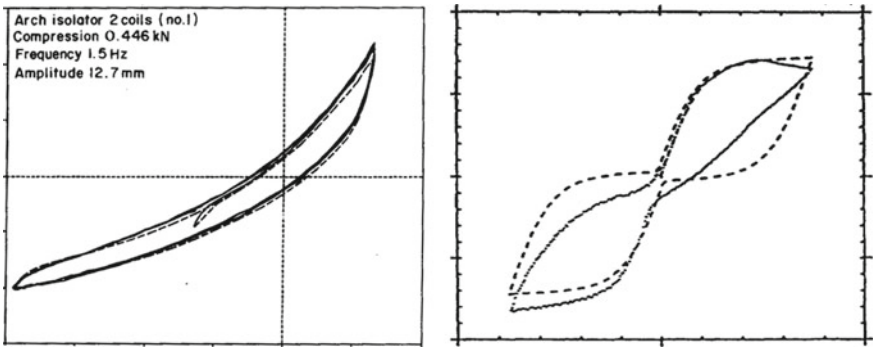

Fig. 7.3 Some asymmetric hysteresis loops obtained in experimental tests. **a** The asymmetric hysteresis behavior of a wire rope isolator along their axial direction—Demetriades et al. (1993). **b** The asymmetric hysteresis behavior of a Nitinol—Dobson et al. (1997)

wire rope isolators deforming along their axial direction (Demetriades et al. 1993) and dampers (Kwok et al. 2006, 2007). Asymmetric hysteresis loops obtained in experimental tests and retrieved from the literature are shown in Fig. 7.3.

7.3.1 Asymmetric Bouc-Wen Models

The differential models described in Sect. 7.2 are not able to reproduce rate-independent asymmetric hysteresis phenomena. Hence, to simulate the typical asymmetric hysteresis loops, some researchers (Sireteanu et al. 2012; Song and Der Kiureghian 2006; Wang and Wen 1998) have proposed the following generalized expression for the function:

$$B = A - |z^n|\,\Psi, \tag{7.8}$$

where Ψ assumes different forms according to the specific improved model that is adopted. In particular, one has

$$\text{Wang and Wen (1998)}: \quad \Psi = \gamma + \beta\ \text{sign}(\dot{x}\ z) + \phi\ \text{sign}(\dot{x} + \dot{z}) \tag{7.9a}$$

$$\text{Song and Der Kiureghian (2006)}: \begin{cases} \Psi = & \beta_1\ \text{sign}(\dot{x}\ z) + \beta_2\ \text{sign}(x\ \dot{x}) \\ & +\beta_3\ \text{sign}(x\ z) + \beta_4\ \text{sign}(\dot{x}) \\ & +\beta_5\ \text{sign}(z) + \beta_6\ \text{sign}(x) \end{cases} \tag{7.9b}$$

$$\text{Sireteanu et al. (2012)}: \begin{cases} \Psi = & \beta_1\ \text{sign}(\dot{x}\ z) + \beta_2\ \text{sign}(x\ \dot{x}) \\ & -\beta_2\ \text{sign}(x\ z) + \beta_4\ \text{sign}(\dot{x}) \\ & +\beta_5\ \text{sign}(z) \end{cases} \tag{7.9c}$$

where $\beta_1, \ldots, \beta_6$ and ϕ are material parameters.

Equation (7.9a), introduced by Wang and Wen, includes an additional parameter ϕ that takes into account the asymmetric behavior; being independent of the sign of the generalized displacement x, Eq. (7.9a) cannot describe the asymmetric hysteresis due to cyclic phenomena since, during them, the sign of the generalized displacement x changes.

For this reason, Song and Der Kiureghian have developed Eq. (7.9b); basically, the function Ψ defined by this equation can assume different values in six phases depending on the signs of x, $\dot{x}$, and z and on the values of six fixed parameters, namely $\beta_1, \ldots, \beta_6$. Consequently, this model has six degrees of freedom that affect the complexity of the parameter identification.

Subsequently, Sireteanu et al. have modified the Song and Der Kiureghian model by imposing the following conditions:

$$\beta_3 = -\beta_2 \quad \text{and} \quad \beta_6 = 0, \tag{7.10}$$

that represent a continuity condition of the hysteresis loop at the points of intersections with the axis of ordinates. Equation (7.9c) describes four different behaviors depending on the signs of x, $\dot{x}$, and z and on the values of only four fixed parameters, namely β_1, β_2, β_4, and β_5.

Figure 7.4 shows the four different curves of the Ψ function defined by Sireteanu et al. The continuity condition (7.10) involves that the hysteretic loop is characterized by the conditions:

$$\Psi_3 = \Psi_4 \quad \text{and} \quad \Psi_6 = \Psi_1. \tag{7.11}$$

Table 7.1 lists the sign combinations of x, $\dot{x}$, and z for the different curves showed in Fig. 7.4.

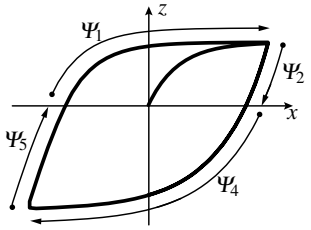

Fig. 7.4 Values of the Ψ function in the model by Sireteanu et al.

Table 7.1 Sign combinations of the Ψ function in the model by Sireteanu et al.

Phase	x	$\dot{x}$	z	$\psi(x, \dot{x}, z)$
1	[−]	+	+	$\psi_1 = \beta_1 + \beta_4 + \beta_5$
2	+	−	+	$\psi_2 = -\beta_1 - 2\beta_2 - \beta_4 + \beta_5$
3	[−]	−	−	$\psi_4 = \beta_1 - \beta_4 - \beta_5$
4	−	+	−	$\psi_5 = -\beta_1 - 2\beta_2 + \beta_4 - \beta_5$

7.3.2 Sensitivity Analysis

A parameter sensitivity analysis was carried out to evaluate the effect of each parameter of the Ψ function on the hysteretic variable $z(x)$ evaluated by adopting Eqs. (7.5), (7.8), and (7.9c).

Figure 7.5 shows the relationship between the hysteretic variable z and the generalized displacement x. All hysteretic loops have been obtained by applying a generalized displacement described by the sine wave (7.7).

The top left plot shows the influence of the first value of the Ψ function, namely Ψ_1, on the hysteretic loop. Such a value modifies the shape of the hysteretic loop in the first and second quadrant when $\dot{x} > 0$ and $z > 0$: the hysteretic variable z is prone to decrease with an increasing value of Ψ_1; the hysteretic loop exhibits work hardening(softening) when the Ψ_1 value is negative (positive).

The influence of the Ψ_2 value on the hysteretic loop is shown in the top right plot. The value Ψ_2 modifies the trend of the hysteretic loop in the second quadrant when $x > 0$, $\dot{x} < 0$, and $z > 0$: the hysteretic variable z is prone to decrease with an increasing value of Ψ_2; the hysteretic loop is concave (convex) when the Ψ_2 value is negative (positive).

The Ψ_4 value modifies the shape of the hysteretic loop in the third and fourth quadrants when $\dot{x} < 0$ and $z < 0$; the influence of such a value is shown in the bottom left plot: the hysteretic variable z is prone to increase with an increasing value of Ψ_4; the hysteretic loop shows work hardening (softening) when the Ψ_4 value is negative (positive).

Finally, the bottom right plot shows the influence of the Ψ_5 value on the hysteretic loop. This value modifies the shape of the hysteretic loop in the third quadrant

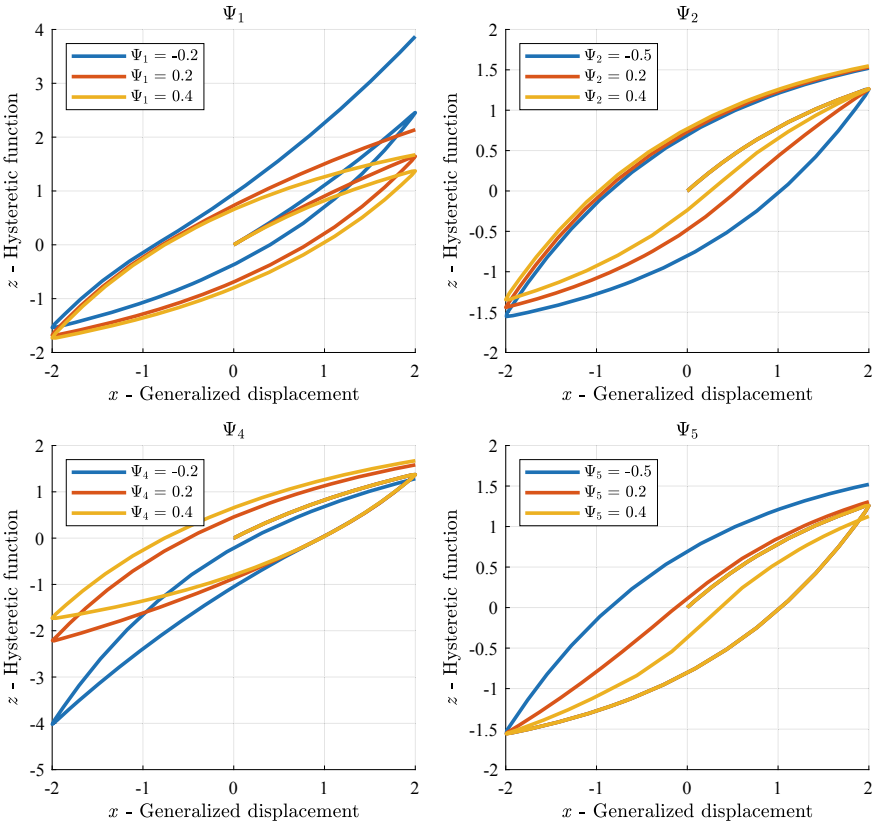

Fig. 7.5 Sensitivity analysis of the model by Sireteanu et al. with respect to the material parameters

when $x < 0$, $\dot{x} > 0$, and $z < 0$: the hysteretic function z is prone to increase with an increasing value of Ψ_5; namely, the hysteretic loop is concave (convex) when the Ψ_5 value is positive (negative).

7.4 Modeling of Pinched Hysteresis Loops

The pinching effect is a physical phenomenon, observed in many experimental results (Kreger and Abrams 1978), in which a very low incremental stiffness near the origin is followed by a stiffening under grater generalized displacements. In particular, we can observe the pinching effect in reinforced concrete structures due to the high shear loads, the slippage of longitudinal reinforcement (Banon and Veneziano 1982), the opening and closing of cracks in the compression zones (Park and Paulay 1975), Y-braced steel frames (Zamani et al. 2012), and confined walls of masonry

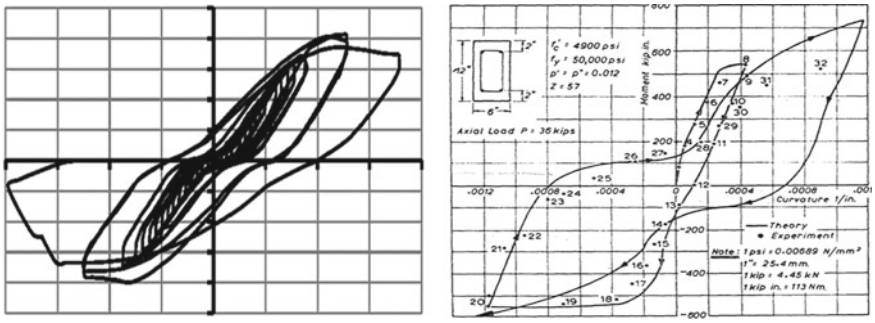

(a) (b)

Fig. 7.6 Some hysteresis loops, having the pinching effect, obtained in experimental tests. **a** The hysteresis behavior of a steel frame having single bays with symmetrical y-shaped concentric bracings—Zamani et al. (2012). **b** The hysteresis behavior of a concrete column section—Park and Paulay (1975)

structures (Ahmad et al. 2012). Some hysteresis loops with the pinching effect, obtained in experimental tests, are shown in Fig. 7.6.

7.4.1 Pinching Bouc-Wen Models

To account for the above-described pinching effects, some researchers (Baber and Noori 1985, 1986; Foliente 1995; Sivaselvan and Reinhorn 2000) have modified the expression of the function employed by the symmetric differential models, described in Sect. 7.2, to evaluate the hysteretic variable z. In particular, some modified expressions of such a function are

$$\text{Baber and Noori (1985):} \begin{cases} B &= \dfrac{B_h\, B_p}{B_h + B_p} \\ B_h &= A - |z^n| \left(\gamma + \beta\ \text{sign}(\dot{x}\, z)\right) \\ B_p &= \left(\dfrac{1}{\sqrt{2\,\pi}\ Z_\sigma}\ \Delta x\ \exp\left(-\dfrac{z^2}{2\, Z_\sigma^2}\right)\right) \end{cases} \tag{7.12a}$$

$$\text{Baber and Noori (1986):} \begin{cases} B &= A\, h - |z^n| \left(\gamma + \beta\ \text{sign}(\dot{x}\, z)\right) \\ h &= 1 - \zeta_1\ \exp\left(-\dfrac{z^2}{2\, \zeta_2^2}\right) \end{cases} \tag{7.12b}$$

Foliente (1995):
$$\begin{cases} B &= A\,h - |z^n|\left(\gamma + \beta\ \mathrm{sign}(\dot{x}\,z)\right) \\ h &= 1 - \zeta_1\ \exp\left(-\dfrac{(z - \bar{z}\ \mathrm{sign}(\dot{x}))^2}{\zeta_2^2}\right) \end{cases} \tag{7.12c}$$

Sivaselvan and Reinhorn (2000):
$$\begin{cases} B &= \dfrac{B_h\,B_p}{B_h + B_p} \\ B_h &= A - \left|\dfrac{z}{z_y}\right|^n \left(\gamma + \beta\ \mathrm{sign}(\dot{x}\,z)\right) \\ B_p &= \left(\dfrac{1}{\sqrt{2\,\pi}\,Z_\sigma}\,\Delta x\,\exp\left(-\dfrac{(z - \bar{z}\ \mathrm{sign}(\dot{x}))^2}{2\,Z_\sigma^2}\right)\right)^{-1} \\ \Delta x &= R_s\,(x_{\max}^{+} - x_{\max}^{-}) \\ Z_\sigma &= \sigma\,z_y \\ \bar{z} &= \lambda\,z_y \end{cases} \tag{7.12d}$$

where B_h, B_p, γ, β, etc. are material parameters.

Baber and Noori (1985) take into account the pinching effect in their model through a pinching spring with stiffness B_p in series with the hysteretic element associated with z, see Eq. (7.12a). The parameter Δx represents the length at which the variable z of the pinching spring tends to $+\infty(-\infty)$, namely:

$$\lim_{x \to +\Delta x^-} z(x) = +\infty, \qquad \lim_{x \to -\Delta x^+} z(x) = -\infty, \tag{7.13}$$

and is associated with the energy dissipation ε. Z_σ is related to the sharpness of pinching; in particular, a higher Z_σ implies a more uniform pinching effect.

In 1986, Baber and Noori proposed a different strategy to account for the pinching effect (see Eq. (7.12b)); in particular, it amounts to multiply the A parameter by a pinching function h that depends on the energy dissipation ε, the hysteretic function z, and two parameters, namely ζ_1 and ζ_2: the first one controls the severity of pinching, whereas the second controls the spread of the pinching region.

Foliente followed the same strategy proposed by Baber and Noori (1986) but proposed a pinching function h that depends on ε, z, ζ_1, and ζ_2, as well as the pinching function h in Eq. (7.12b); in addition, the function h also depends on the parameter $\bar{z}$ that corresponds to a fraction of z at $\mathrm{d}z/\mathrm{d}x = 0$.

Finally, Sivaselvan and Reinhorn proposed a model similar to the one by Baber and Noori (1985), the main difference lying in the fact that in the former model the pinching parameter Δx depends on the maximum generalized displacement reached on the positive and negative sides during the response, weighed through the parameter of the model R_s, and no longer on the energy dissipation ε. Z_σ and $\bar{z}$ are two variables that depend on the yield value of the hysteretic variable, i.e. z_y through two parameters of the model, namely σ and λ (see Eq. (7.12d)).

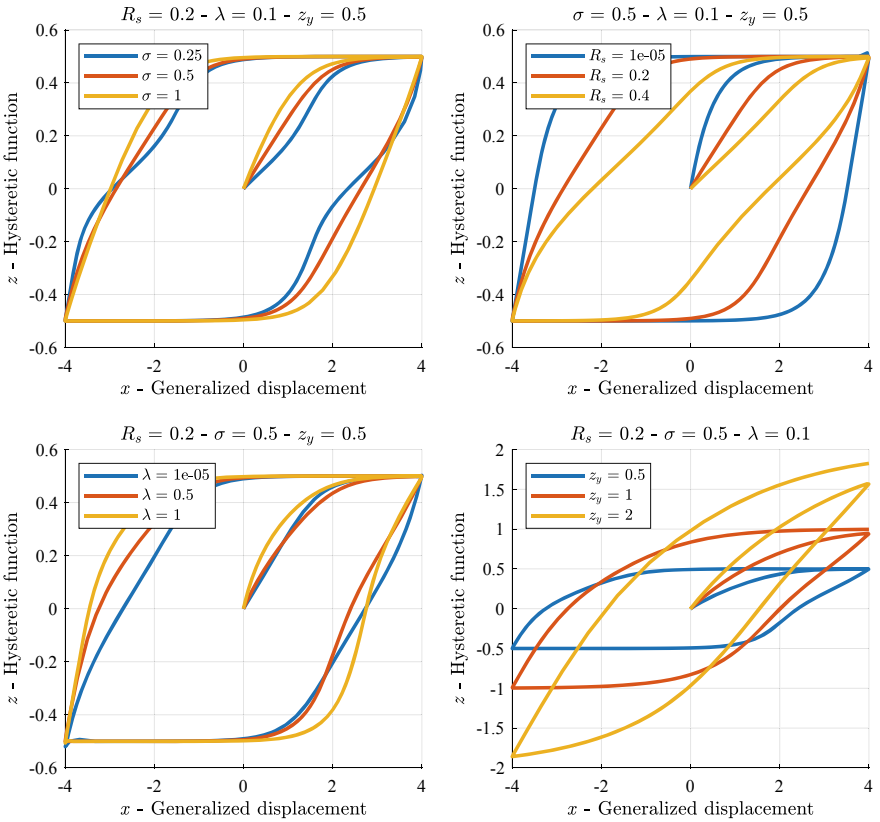

Fig. 7.7 Sensitivity analysis of Sivaselvan and Reinhorn model parameters

7.4.2 Sensitivity Analysis

A sensitivity analysis was carried out to evaluate the effect of each parameter on the hysteretic variable $z(t)$ evaluated by adopting Eqs. (7.5) and (7.12d). The effects of the parameters R_s, σ, λ, and z_y on the hysteretic function z are shown in Fig. 7.7. All hysteretic loops have been obtained by applying a generalized displacement described by the sine wave (7.7).

The top left plot shows the variation of the σ parameter: this parameter controls the pinching region and increasing σ causes the pinching region to spread. The top right plot shows the variation of the R_s parameter: the intensity of the pinching effect is prone to decrease with a decreasing R_s; specifically, when R_s approaches 0, the pinching effect is null. The bottom left plot shows the variations of the λ parameter: the hysteresis loop tends to become more asymmetric when λ increases. Finally, the bottom right plot shows the variation of the z_y parameter: the tangent stiffness at the origin of the hysteresis loop increases with an increasing value of z_y.

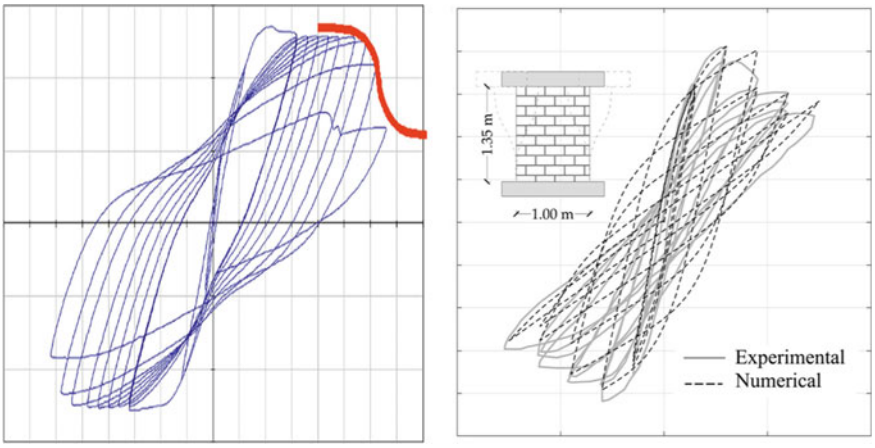

(a) (b)

Fig. 7.8 Hysteresis loops with the pinching effect obtained from experimental tests. **a** The hysteresis behaviour of a well confined reinforced concrete column—Colombo and Negro (2005). **b** The hysteresis behavior of a unreinforced masonry panels—Liberatore et al. (2019)

7.5 Modeling of Degrading Hysteresis Loops

It is well known from the scientific literature that many mechanical systems can exhibit strength and stiffness degradation. In general, we can see a hysteretic degrading behavior when the systems are subjected to cyclic loads like earthquakes, winds, and so on. For instance, in concrete (Loh et al. 2011; Sengupta and Li 2013, 2014) and masonry (Liberatore et al. 2019; Tomaževič and Lutman 1996) structures, it is possible to observe a progressive loss of stiffness due to the opening and closing of cracks when the applied loads change direction. Wooden structures also exhibit hysteretic degrading behavior (Xu and Dolan 2009; Zhang et al. 2002). In Fig. 7.8, hysteresis loops exhibiting strength and stiffness degradation are shown.

7.5.1 Degrading Bouc-Wen Models

Similar to the asymmetric and pinched hysteresis phenomena, several researchers (Baber and Wen 1981; Baber and Noori 1985; Foliente 1995) have modified the differential models described in Sect. 7.2 to allow for the simulation of the stiffness and strength degradation effects. Specifically, they have modified the expression employed for evaluating the hysteresis function, required to compute the model output, as follows:

$$\text{Baber and Wen (1981):} \quad \begin{cases} B &= \dfrac{A}{\eta} - \nu\,|z^n|\left(\gamma + \beta\ \text{sign}(\dot{x}\,z)\right) \\ A &= A[\varepsilon(t)] = A_0 - \delta_A\,\varepsilon(t) \\ \eta &= \eta[\varepsilon(t)] = \eta_0 + \delta_\eta\,\varepsilon(t) \\ \nu &= \nu[\varepsilon(t)] = \nu_0 + \delta_\nu\,\varepsilon(t) \end{cases} \tag{7.14a}$$

$$\text{Baber and Noori (1985):} \quad \begin{cases} B &= \dfrac{A}{\eta} - \nu\,|z^n|\left(\gamma + \beta\ \text{sign}(\dot{x}\,z)\right) \\ A &= A[\varepsilon(t)] = A_0 - \delta_A\,\varepsilon(t) \\ \eta &= \eta[\varepsilon(t)] = 1 + \delta_\eta\,\varepsilon(t) \\ \nu &= \nu[\varepsilon(t)] = 1 + \delta_\nu\,\varepsilon(t) \end{cases} \tag{7.14b}$$

$$\text{Foliente (1995)}: \quad \begin{cases} B &= \dfrac{A}{\eta} - \nu\,|z^n|\left(\gamma + \beta\ \text{sign}(\dot{x}\,z)\right) \\ \eta &= \eta[\varepsilon(t)] = 1 + \delta_\eta\,\varepsilon(t) \\ \nu &= \nu[\varepsilon(t)] = 1 + \delta_\nu\,\varepsilon(t) \end{cases} \tag{7.14c}$$

where A, η, ν, etc. are material parameters.

All models consider strength, stiffness, or combined degradation, from the initial time $t = 0$ to the present one, as a function of the dissipated energy associated with the hysteretic displacement z; its expression is given by

$$\varepsilon(t) = \int_0^t z\,\dot{x}\,\mathrm{d}\,t. \tag{7.15}$$

In particular, a convenient measure of degradation is the cumulative hysteretic dissipated energy $\varepsilon(t)$ since degradation depends on the intensity and duration of the phenomenon under investigation.

Baber and Wen defined two new parameters: η and ν controlling in turn the stiffness and the strength degradation. Moreover, the amplitude of the hysteresis loop, controlled by the A parameter, can change. In the Baber and Noori 1985 model, the η_0 and ν_0 parameters, which represent the initial values of the degradation functions, are set to 1. Finally, in the Foliente model, the degradation law related to the A parameter is null. All models assume that both parameters η and ν depend linearly on the hysteretic energy $\varepsilon(t)$.

It is worth being emphasized that the energy dissipated by the material coincides with $\varepsilon(t)$ in Eq. (7.15) only for peculiar values of the parameters. In general, $\varepsilon(t)$ does not necessarily fulfill the thermodynamic compatibility (Drucker 1957). For this reason, the use of degrading Bouc-Wen formulations should carefully account for such an issue.

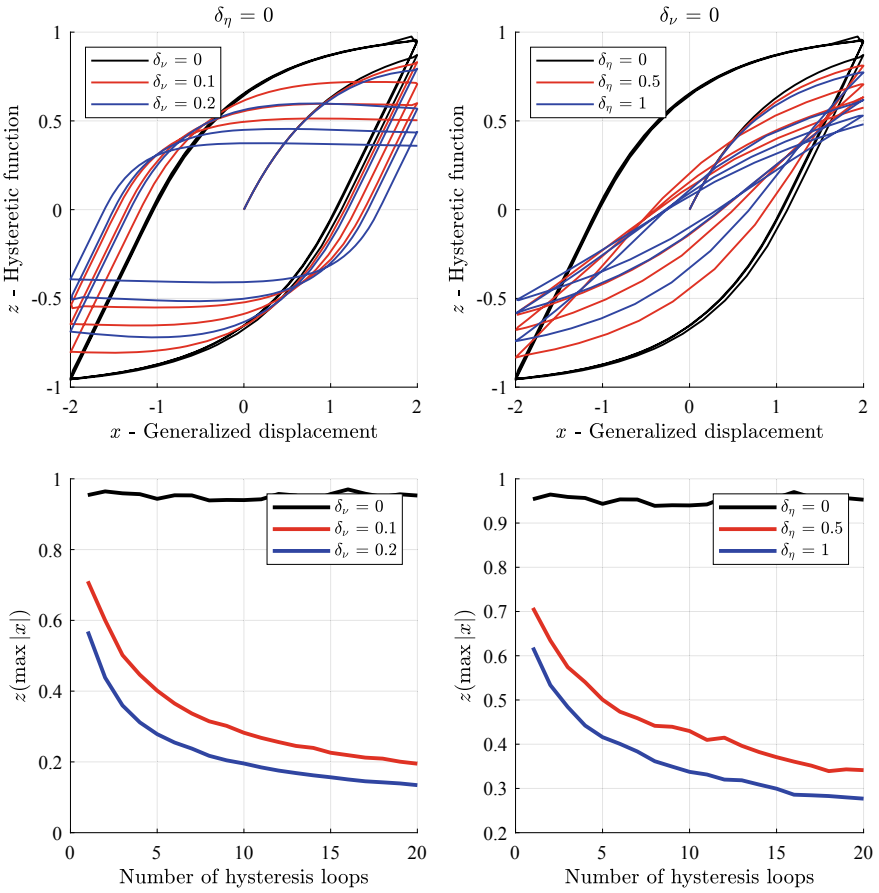

Fig. 7.9 Sensitivity analysis of Foliente model parameters

7.5.2 Sensitivity Analysis

Sensitivity analysis has been carried out on the Foliente model (Foliente 1995) and the results are shown in Fig. 7.9. The top left and the top right plots show the hysteresis loops that exhibit a strength and stiffness degradation, respectively. For both top plots, there are two black colored hysteresis loops without any kind of degradation, obtained by setting to zero the values of δ_η and δ_ν. Conversely, when the latter parameters are greater than zero, a degrading hysteretic behavior is obtained; in particular, the rate of the strength and stiffness degradation gets stronger when the δ_η and δ_ν parameters, respectively, increase. All hysteretic loops have been obtained by applying a generalized displacement described by the sine wave (7.7).

The two bottom plots show the relationship between the number of hysteresis loops and the value of the hysteretic function z associated with the maximum positive

displacement x. In these plots, the effect of δ_η and δ_ν parameters on the hysteresis behavior is more evident.

7.6 Conclusion

Over the years, the Bouc-Wen model has evolved to describe some physical phenomena observed in experimental tests. In this paper, the evolution of the Bouc-Wen model in the field of *rate-independent* mechanical hysteresis phenomena has been presented. In particular, we have reviewed some models based on the Bouc-Wen model able to take into account some mechanical phenomena such as asymmetric hysteresis, the pinching effect, and the strength and stiffness degradation of hysteresis. In all sections, we have used the same technical terminology to help the reader to get acquainted with the physical meaning of the proposed models, to compare each model, and to shed light on their differences, such as the number of parameters that the models require as input.

Finally, for all models, some sensitivity analyses have been carried out to evaluate the effect on the model's result when the input parameters are modified.

References

Ahmad N, Ali Q, Ashraf M, Khan AN, Alam B (2012) Performance assessment of low-rise confined masonry structures for earthquake induced ground motions. Int J Civil Struct Eng 2(3):842–859

Alibert JJ, Seppecher P, dell'Isola F (2003) Truss modular beams with deformation energy depending on higher displacement gradients. Math Mech Solids 8(1):51–73

Altenbach H, Bîrsan M, Eremeyev VA (2012) On a thermodynamic theory of rods with two temperature fields. Acta Mech 223(8):1583–1596

Andreaus U, Spagnuolo M, Lekszycki T, Eugster SR (2018) A Ritz approach for the static analysis of planar pantographic structures modeled with nonlinear Euler-Bernoulli beams. Contin Mech Thermodyn 30(5):1103–1123

Ascione L, Berardi V, Feo L, Fraternali F, Tralli AM (2017) Probabilistic assessment of historical masonry walls retrofitted with through-the-thickness confinement devices. Proc AIMETA

Baber TT, Noori MN (1985) Random vibration of degrading, pinching systems. J Eng Mech 111(8):1010–1026

Baber TT, Noori MN (1986) Modeling general hysteresis behavior and random vibration application. J Vibr Acoust Stress Rel Des

Baber TT, Wen YK (1981) Random vibration of hysteretic, degrading systems. J Eng Mech Div 107(6):1069–1087

Badoni D, Makris N (1996) Nonlinear response of single piles under lateral inertial and seismic loads. Soil Dyn Earthq Eng 15(1):29–43

Bahn BY, Hsu CTT (1998) Stress-strain behavior of concrete under cyclic loading. ACI Mater J 95:178–193

Bai XX, Cai FL, Chen P (2019) Resistor-capacitor (RC) operator-based hysteresis model for magnetorheological (MR) dampers. Mech Syst Signal Process 117:157–169

Banon H, Veneziano D (1982) Seismic safety of reinforced concrete members and structures. Earthq Eng Struct Dyn 10(2):179–193

Barchiesi E, dell'Isola F, Laudato M, Placidi L, Seppecher P (2018) A 1d continuum model for beams with pantographic microstructure: asymptotic micro-macro identification and numerical results. In: Advances in mechanics of microstructured media and structures. Springer, pp 43–74

Barchiesi E, Eugster SR, dell'Isola F, Hild F (2020) Large in-plane elastic deformations of bi-pantographic fabrics: asymptotic homogenization and experimental validation. Math Mech Solids 25(3):739–767

Bouc R (1967) Forced vibrations of mechanical systems with hysteresis. In: Proceedings of the fourth conference on nonlinear oscillations, Prague

Bouc R (1971) Modèle mathématique d'hystérésis. Acustica 21:16–25

Broccardo M, Alibrandi U, Wang Z, Garrè L (2017) The tail equivalent linearization method for nonlinear stochastic processes, genesis and developments. In: Risk and reliability analysis: theory and applications. Springer, pp 109–142

Caggegi C, Sciuto D, Cuomo M (2018) Experimental study on effective bond length of basalt textile reinforced mortar strengthening system: contributions of digital image correlation. Measurement 129:119–127

Carboni B, Lacarbonara W, Brewick PT, Masri SF (2018) Dynamical response identification of a class of nonlinear hysteretic systems. J Intell Mater Syst Struct 29(13):2795–2810

Colombo A, Negro P (2005) A damage index of generalised applicability. Eng Struct 27(8):1164–1174

Contrafatto L, Cuomo M (2002) A new thermodynamically consistent continuum model for hardening plasticity coupled with damage. Int J Solids Struct 39(25):6241–6271

Contrafatto L, Cuomo M, Fazio F (2012) An enriched finite element for crack opening and rebar slip in reinforced concrete members. Int J Fract 178(1–2):33–50

di Cosmo F, Laudato M, Spagnuolo M (2018) Acoustic metamaterials based on local resonances: homogenization, optimization and applications. In: Generalized models and non-classical approaches in complex materials 1. Springer, pp 247–274

De Angelo M, Spagnuolo M, D'annibale F, Pfaff A, Hoschke K, Misra A, Dupuy C, Peyre P, Dirrenberger J, Pawlikowski M (2019) The macroscopic behavior of pantographic sheets depends mainly on their microstructure: experimental evidence and qualitative analysis of damage in metallic specimens. Contin Mech Thermodyn 31(4):1181–1203

dell'Isola F, Seppecher P, Alibert JJ, Lekszycki T, Grygoruk R, Pawlikowski M, Steigmann D, Giorgio I, Andreaus U, Turco E et al (2019a) Pantographic metamaterials: an example of mathematically driven design and of its technological challenges. Contin Mech Thermodyn 31(4):851–884

dell'Isola F, Turco E, Misra A, Vangelatos Z, Grigoropoulos C, Melissinaki V, Farsari M (2019b) Force-displacement relationship in micro-metric pantographs: experiments and numerical simulations. Comptes Rendus Mécanique 347(5):397–405

Demetriades GF, Constantinou MC, Reinhorn AM (1993) Study of wire rope systems for seismic protection of equipment in buildings. Eng Struct 15(5):321–334

Dimian M, Andrei P (2014) Noise-driven phenomena in hysteretic systems. Springer

Dobson S, Noori M, Hou Z, Dimentberg M, Baber T (1997) Modeling and random vibration analysis of SDOF systems with asymmetric hysteresis. Int J Non-Linear Mech 32(4):669–680

Drucker DC (1957) A definition of stable inelastic material. BROWN UNIV PROVIDENCE RI, Tech. rep

Duhem P (1897) Die dauernden aenderungen und die thermodynamik. i. Zeitschrift für Physikalische Chemie 22(1):545–589

Eremeyev V, Morozov N (2010) The effective stiffness of a nanoporous rod. Dokl Phys 55:279–282

Fedele R, Sessa S, Valoroso N (2012) Image correlation-based identification of fracture parameters for structural adhesives. Technische Mechanik-Europ J Eng Mech 32(2–5):195–204

Foliente GC (1995) Hysteresis modeling of wood joints and structural systems. J Struct Eng 121(6):1013–1022

Fujimura K, Der Kiureghian A (2007) Tail-equivalent linearization method for nonlinear random vibration. Probab Eng Mech 22(1):63–76

Graesser E, Cozzarelli F (1991) Shape-memory alloys as new materials for aseismic isolation. J Eng Mech 117(11):2590–2608
Greco F, Luciano R, Serino G, Vaiana N (2018) A mixed explicit-implicit time integration approach for nonlinear analysis of base-isolated structures. Annals Solid Struct Mech 10(1):17–29
Greco L, Cuomo M (2013) B-Spline interpolation of Kirchhoff-love space rods. Comput Methods Appl Mech Eng 256:251–269
Hadad HA, Calabrese A, Strano S, Serino G (2017) A base isolation system for developing countries using discarded tyres filled with elastomeric recycled materials. J Earthq Eng 21(2):246–266
Hodgdon ML (1988) Mathematical theory and calculations of magnetic hysteresis curves. IEEE Trans Magn 24(6):3120–3122
Hossain MM, Browning R, Minkwitz R, Sue HJ (2012) Effect of asymmetric constitutive behavior on scratch-induced deformation of polymers. Tribol Lett 47(1):113–122
Jiles D, Atherton D (1983) Ferromagnetic hysteresis. IEEE Trans Magn 19(5):2183–2185
Jiles DC, Atherton DL (1984) Theory of ferromagnetic hysteresis. J Appl Phys 55(6):2115–2120
Kikuchi M, Aiken ID (1997) An analytical hysteresis model for elastomeric seismic isolation bearings. Earthq Eng Struct Dyn 26(2):215–231
Kreger ME, Abrams DP (1978) Measured hysteresis relationships for small-scale beam-column joints. Tech. rep., University of Illinois Engineering Experiment Station. College of
Kwok N, Ha Q, Nguyen T, Li J, Samali B (2006) A novel hysteretic model for magnetorheological fluid dampers and parameter identification using particle swarm optimization. Sens Actuators, A 132(2):441–451
Kwok N, Ha Q, Nguyen M, Li J, Samali B (2007) Bouc-wen model parameter identification for a MR fluid damper using computationally efficient GA. ISA Trans 46(2):167–179
Liberatore D, Addessi D, Sangirardi M (2019) An enriched Bouc-Wen model with damage. Europ J Mech-A/Solids 77(103):771
Lima C, Angiolilli M, Barbagallo F, Belletti B, Bergami A, Camata G, Cantagallo C, Di Domenico M, Fiorentino G, Ghersi A, et al (2018) Nonlinear modeling approaches for existing reinforced concrete buildings: The case study of de gasperi-battaglia school building in norcia. In: Conference on Italian concrete days. Springer, pp 82–95
Loh CH, Mao CH, Huang JR, Pan TC (2011) System identification and damage evaluation of degrading hysteresis of reinforced concrete frames. Earthq Eng Struct Dyn 40(6):623–640
Losanno D, Sierra IEM, Spizzuoco M, Marulanda J, Thomson P (2019a) Experimental assessment and analytical modeling of novel fiber-reinforced isolators in unbounded configuration. Compos Struct 212:66–82
Losanno D, Spizzuoco M, Calabrese A (2019b) Bidirectional shaking-table tests of unbonded recycled-rubber fiber-reinforced bearings (rr-frbs). Struct Control Health Monit 26(9)
Losanno D, Palumbo F, Calabrese A, Barrasso T, Vaiana N (2021) Preliminary investigation of aging effects on recycled rubber fiber reinforced bearings (RR-FRBs). J Earthq Eng, 1–18
Marmo F, Rosati L (2012a) Analytical integration of elasto-plastic uniaxial constitutive laws over arbitrary sections. Int J Numer Meth Eng 91(9):990–1022
Marmo F, Rosati L (2012b) An improved flexibility-based nonlinear frame element endowed with the fiber-free formulation. European congress on computational methods in applied sciences and engineering (ECCOMAS 2012). Viena, Austria, pp 1–17
Marmo F, Rosati L (2013) The fiber-free approach in the evaluation of the tangent stiffness matrix for elastoplastic uniaxial constitutive laws. Int J Numer Meth Eng 94(9):868–894
Marmo F, Serpieri R, Rosati L (2011) Ultimate strength analysis of prestressed reinforced concrete sections under axial force and biaxial bending. Comput Struct 89(1–2):91–108
Mayergoyz ID (2003) Mathematical models of hysteresis and their applications. Academic Press
Menegotto M (1973) Method of analysis for cyclically loaded RC plane frames including changes in geometry and non-elastic behavior of elements under combined normal force and bending. In: Proc. of IABSE symposium on resistance and ultimate deformability of structures acted on by well defined repeated loads, pp 15–22

Nejadsadeghi N, De Angelo M, Drobnicki R, Lekszycki T, dell'Isola F, Misra A (2019) Parametric experimentation on pantographic unit cells reveals local extremum configuration. Exp Mech 59(6):927–939

Noël JP, Kerschen G (2017) Nonlinear system identification in structural dynamics: 10 more years of progress. Mech Syst Signal Process 83:2–35

Nuzzo I, Losanno D, Caterino N, Serino G, Rotondo LMB (2018) Experimental and analytical characterization of steel shear links for seismic energy dissipation. Eng Struct 172:405–418

Nuzzo I, Losanno D, Caterino N (2019) Seismic design and retrofit of frame structures with hysteretic dampers: a simplified displacement-based procedure. Bull Earthq Eng 17(5):2787–2819

Özdemir H (1976) Nonlinear transient dynamic analysis of yielding structures[ph. d. thesis]. PhD thesis, University of California

Park R, Paulay T (1975) Reinforced concrete structures. John Wiley & Sons

Pellecchia D, Sessa S, Vaiana N, Rosati L (2020) Comparative assessment on the rocking response of seismically base-isolated rigid blocks. Proc Struct Integrity 29:95–102

Pideri C, Seppecher P (1997) A second gradient material resulting from the homogenization of an heterogeneous linear elastic medium. Continuum Mech Thermodyn 9(5):241–257

Placidi L, Barchiesi E, Misra A (2018) A strain gradient variational approach to damage: a comparison with damage gradient models and numerical results. Math Mech Complex Syst 6(2):77–100

Placidi L, Misra A, Barchiesi E (2019) Simulation results for damage with evolving microstructure and growing strain gradient moduli. Continuum Mech Thermodyn 31(4):1143–1163

Ramberg W, Osgood WR (1943) Description of stress-strain curves by three parameters. Nat Adv Committ Aeron

Sengupta P, Li B (2013) Modified Bouc-wen model for hysteresis behavior of RC beam-column joints with limited transverse reinforcement. Eng Struct 46:392–406

Sengupta P, Li B (2014) Hysteresis behavior of reinforced concrete walls. J Struct Eng 140(7):04014,030

Serpieri R, Sessa S, Rosati L (2018) A MITC-based procedure for the numerical integration of a continuum elastic-plastic theory of through-the-thickness-jacketed shell structures. Compos Struct 191:209–220

Sessa S (2010) Multiobjective non-linear random vibration analysis for performance-based earthquake engineering. Reliability and optimization of structural systems-proceedings of reliability and optimization of structural systems pp 185–192

Sessa S, Valoroso N (2017) Kriging interpolation strategy for finite-element-based surrogate responses of DCB delamination tests. In: Risk and reliability analysis: theory and applications. Springer, pp 453–461

Sessa S, Serpieri R, Rosati L (2017) A continuum theory of through-the-thickness jacketed shells for the elasto-plastic analysis of confined composite structures: theory and numerical assessment. Compos B Eng 113:225–242

Sessa S, Marmo F, Rosati L, Leonetti L, Garcea G, Casciaro R (2018) Evaluation of the capacity surfaces of reinforced concrete sections: eurocode versus a plasticity-based approach. Meccanica 53(6):1493–1512

Sessa S, Marmo F, Vaiana N, De Gregorio D, Rosati L (2019a) Strength hierarchy provisions for transverse confinement systems of shell structural elements. Compos B Eng 163:413–423

Sessa S, Marmo F, Vaiana N, Rosati L (2019b) Probabilistic assessment of axial force-biaxial bending capacity domains of reinforced concrete sections. Meccanica 54(9):1451–1469

Sessa S, Vaiana N, Paradiso M, Rosati L (2020) An inverse identification strategy for the mechanical parameters of a phenomenological hysteretic constitutive model. Mech Syst Signal Process 139(106):622

Shih MH, Sung WP (2005) A model for hysteretic behavior of rhombic low yield strength steel added damping and stiffness. Comput Struct 83(12–13):895–908

Sierra IEM, Losanno D, Strano S, Marulanda J, Thomson P (2019) Development and experimental behavior of HDR seismic isolators for low-rise residential buildings. Eng Struct 183:894–906

Sireteanu T, Giuclea M, Mitu AM, Ghita G (2012) A genetic algorithms method for fitting the generalized bouc-wen model to experimental asymmetric hysteretic loops. J Vib Acoust 134(4)
Sivaselvan MV, Reinhorn AM (2000) Hysteretic models for deteriorating inelastic structures. J Eng Mech 126(6):633–640
Song J, Der Kiureghian A (2006) Generalized Bouc-wen model for highly asymmetric hysteresis. J Eng Mech 132(6):610–618
Song J, Kiureghian AD, Sackman JL (2007) Seismic interaction in electrical substation equipment connected by non-linear rigid bus conductors. Earthq Eng Struct Dyn 36(2):167–190
Tomaževič M, Lutman M (1996) Seismic behavior of masonry walls: modeling of hysteretic rules. J Struct Eng 122(9):1048–1054
Turco E, Giorgio I, Misra A, dell'Isola F (2017) King post truss as a motif for internal structure of (meta) material with controlled elastic properties. Royal Soc Open Sci 4(10):171,153
Turco E, Misra A, Pawlikowski M, dell'Isola F, Hild F (2018) Enhanced Piola-Hencky discrete models for pantographic sheets with pivots without deformation energy: numerics and experiments. Int J Solids Struct 147:94–109
Vaiana N, Spizzuoco M, Serino G (2017) Wire rope isolators for seismically base-isolated lightweight structures: experimental characterization and mathematical modeling. Eng Struct 140:498–514
Vaiana N, Sessa S, Marmo F, Rosati L (2018) A class of uniaxial phenomenological models for simulating hysteretic phenomena in rate-independent mechanical systems and materials. Nonlinear Dyn 93(3):1647–1669
Vaiana N, Sessa S, Marmo F, Rosati L (2019a) An accurate and computationally efficient uniaxial phenomenological model for steel and fiber reinforced elastomeric bearings. Compos Struct 211:196–212
Vaiana N, Sessa S, Marmo F, Rosati L (2019b) Nonlinear dynamic analysis of hysteretic mechanical systems by combining a novel rate-independent model and an explicit time integration method. Nonlinear Dyn 98(4):2879–2901
Vaiana N, Sessa S, Paradiso M, Marmo F, Rosati L (2019c) An efficient computational strategy for nonlinear time history analysis of seismically base-isolated structures. In: Conference of the Italian association of theoretical and applied mechanics. Springer, pp 1340–1353
Vaiana N, Sessa S, Paradiso M, Rosati L (2019d) Accurate and efficient modeling of the hysteretic behavior of sliding bearings. In: 7th international conference on computational methods in structural dynamics and earthquake engineering (COMPDYN 2019). Crete, Greece, pp 24–26
Vaiana N, Marmo F, Sessa S, Rosati L (2020) Modeling of the hysteretic behavior of wire rope isolators using a novel rate-independent model. Nonlinear Dynamics of Structures. Springer, Systems and Devices, pp 309–317
Vaiana N, Capuano R, Sessa S, Marmo F, Rosati L (2021a) Nonlinear dynamic analysis of seismically base-isolated structures by a novel opensees hysteretic material model. Appl Sci 11(3):900
Vaiana N, Losanno D, Ravichandran N (2021b) A novel family of multiple springs models suitable for biaxial rate-independent hysteretic behavior. Comput Struct 244(106):403
Vaiana N, Sessa S, Rosati L (2021c) A generalized class of uniaxial rate-independent models for simulating asymmetric mechanical hysteresis phenomena. Mech Syst Signal Process 146(106):984
Valoroso N, Fedele R (2010) Characterization of a cohesive-zone model describing damage and de-cohesion at bonded interfaces. sensitivity analysis and mode-i parameter identification. International Journal of Solids and Structures 47(13):1666–1677
Valoroso N, Sessa S, Lepore M, Cricri G (2013) Identification of mode-i cohesive parameters for bonded interfaces based on DCB test. Eng Fract Mech 104:56–79
Valoroso N, Marmo F, Sessa S (2014) Limit state analysis of reinforced shear walls. Eng Struct 61:127–139
Valoroso N, Marmo F, Sessa S (2015) A novel shell element for nonlinear pushover analysis of reinforced concrete shear walls. Bull Earthq Eng 13(8):2367–2388
Visintin A (2013) Differential models of hysteresis, vol 111. Springer Science & Business Media

Wang CH, Wen Yk (1998) Reliability and redundancy of pre-Northridge low-rise steel buildings under seismic excitation. na

Wen Y (1980) Equivalent linearization for hysteretic systems under random excitation. ASME J Appl Mech

Wen YK (1976) Method for random vibration of hysteretic systems. J Eng Mech Div 102(2):249–263

Xu J, Dolan JD (2009) Development of a wood-frame shear wall model in abaqus. J Struct Eng 135(8):977–984

Zamani SM, Vafai A, Aghakouchak A, Kazemi M (2012) Experimental investigation of steel frames with single bays of symmetrical y-shaped concentric bracings. Scientia Iranica 19(2):195–210

Zhang H, Foliente GC, Yang Y, Ma F (2002) Parameter identification of inelastic structures under dynamic loads. Earthq Eng Struct Dyn 31(5):1113–1130

Zuccaro G, Dato F, Cacace F, De Gregorio D, Sessa S (2017) Seismic collapse mechanisms analyses and masonry structures typologies: a possible correlation. Ingegneria Sismica 34(4):121–150